Nano Today xxx (xxxx) xxx

Contents lists available at ScienceDirect

Nano Today

journal homepage: www.elsevier.com/locate/nanotoday

Rapid communication

Temperature dependence of the pyro-phototronic effect in self-powered p-Si/n-ZnO nanowires heterojuncted ultraviolet sensors

Jianqi Dong [a], Zhengjun Wang [b], Xingfu Wang [a,b,*], Zhong Lin Wang [b,c,*]

[a] Laboratory of Nanophotonic Functional Materials and Devices, Guangdong Engineering Technology Research Center of Optoelectronic Functional Materials and Devices, Institute of Optoelectronic Materials and Technology, South China Normal University, Guangzhou, 510631, China
[b] School of Materials Science and Engineering, Georgia Institute of Technology, Atlanta, GA, 30332-0245, USA
[c] Beijing Institute of Nanoenergy and Nanosystems, Chinese Academy of Sciences, Beijing, 100083, China

ARTICLE INFO

Article history:
Received 27 May 2019
Received in revised form
10 September 2019
Accepted 30 September 2019
Available online xxx

Keywords:
Temperature
pn junction
The pyro-phototronic effect
UV sensors

ABSTRACT

Self-powered pn-juncted devices fabricated with pyroelectric semiconductor have attached much attention as active ultraviolet (UV) photodetectors (PDs), featuring with energy-efficient, active functionality and ultrafast response speed. Herein, the pyroelectric ZnO nanowires (NWs) grown on p-Si are functioned as a self-powered UV PD. Without an external voltage, the fabricated device exhibits a stable and uniform UV sensing ability with high photoresponsivity and fast response and decay time. Furthermore, the effects of ambient temperature on the self-powered UV PD are systematically investigated. Under the temperature of 77 K, the current response of the UV PD is significantly improved by over 1304%, while it is only increased by 532.6% at RT. Under the temperatures above RT, the UV PD functions well in a self-powering and stable manner even the temperature is elevated to 85 °C from RT, exhibiting good photoresponsivity of 17.0 mA/W and fast response time of 700 μs at the rise edge. By analyzing energy diagrams of the pn junction, the underlying physical mechanism of the self-powered UV PDs is carefully illustrated. This study provides guiding significance for research of high-performances UV sensing and ultrafast optoelectronic communication.

Introduction

Ultraviolet Photodetectors (UV PDs) have drawn considerable attention owing to their wide-range applications in industrial and scientific fields, including flame warning [1], pollutant monitoring [2,3], water purification and personal protection [4–6]. Various UV PDs featuring high responsivity, large detectivity and fast response and/or recovery speed, have been intensively investigated in the past decades based on many semiconductors with different structures (such as films, nanowires and nanoparticals) [7–12]. However, for most of the reported UV PDs, their excellent detecting performances or even normal operation relies heavily on the external power supplying [13–16]. This has long been an obstacle to meet the growing industrial requirements of UV PDs in terms of cost-saving, energy-efficiency and size minimization. Therefore, newly designed UV PDs with self-powering capability, which could function well in a sustainable, high regularity and less maintenance manner without external power supplying, may become necessary. In the absence of external applied voltage, the intrinsic and/or self-generating electric field that can act as an effective actuating force for separation of electron-hole pairs and transportation of the charge carriers, is a critical point to fabricate a self-powered UV PDs. In addition, Silicon (Si)-based UV senors still need to be improved in terms of the power-consumption and photoresponse performances, although Si has been the cornerstone of modern integrated circuit technology. It is of great significance to develop a low-cost and self-powered Si-based UV sensor for improving the technology of low-power monolithic-integrated system.

For pyroelectric semiconductors with non-centrosymmetric crystal structures, such as *c*-axis ZnO nanowires (NWs), the pyroelectric polarization field would be generated by time-dependently changing temperature across the semiconductors. In the case of UV detecting, the temperature of ZnO NWs would be speedily increased upon UV light illuminations, resulting in the generation of pyroelectric polarization field (E_{py}) along *c*-axics of ZnO NWs with a distribution of pyroelectric charges at both ends of the NWs [17–19]. This light-induced pyroelectric polarization field is actually a self-generating electric field that can realize the self-powered

* Corresponding authors at: School of Materials Science and Engineering, Georgia Institute of Technology, Atlanta, GA, 30332-0245, USA.
E-mail addresses: xf.wang@m.scnu.edu.cn (X. Wang), zhong.wang@mse.gatech.edu (Z.L. Wang).

https://doi.org/10.1016/j.nantod.2019.100798
1748-0132/

Please cite this article as: J. Dong, Z. Wang, X. Wang et al., Temperature dependence of the pyro-phototronic effect in self-powered p-Si/n-ZnO nanowires heterojuncted ultraviolet sensors, Nano Today, https://doi.org/10.1016/j.nantod.2019.100798

functionality in ZnO NW-based devices with proper design. Moreover, the E_{py} can quickly and effectively modulate the charge transport and distribution inside the semiconductor material, readjust the energy band diagrams, and thus optimize the performance of the semiconductor optoelectronic device. This is referred to as the pyro-phototronic effect [20–24]. Considering that the temperature and its variation within ZnO NWs is the core of the induced pyroelectric polarization field, the effects of ambient temperature on the self-powered UV sensors induced by the pyro-phototronic effect is essential for improving their practical applications.

In this work, the pyroelectric ZnO NWs hydrothermally grown on p-Si substrate, are utilized to form a p-n junction for functional application as an UV PD. Without the external voltage, the fabricated device exhibits a stable and uniform UV sensing ability with high photoresponsivity and fast response and decay time. Furthermore, the effects of ambient temperature on the p-Si/n-ZnO NWs self-powered UV PD are systematically investigated under the temperatures above room temperature (RT) ranging from 25 to 85 °C and below RT ranging from 300 to 77 K. Under the temperature below RT, the current response of the UV PD is significantly improved by over 1304%, while at RT the current response is only increased by 532.6% induced by introducing the pyroelectric effect. Under the temperatures above RT, the UV PD functions well even the temperature is elevated to 85 °C from RT. And the increasing of temperature between RT to 85 °C results in, to some extent, performances declination in the UV detector. By analyzing energy diagrams of the p-Si/n-ZnO heterojunction, the working principle of pyro-phototronic effect is carefully illustrated. The relationship between the performance of the sensors and the temperature and light intensities has been studied in depth, which has guiding significance for the research of high-performances UV sensing, ultrafast optoelectronic communication, and flame/temperature monitoring. This work provides in-depth understandings about the temperature-dependence of the pyro-phototronic effect and indicates huge potential of the self-powered UV sensor in Si-based optoelectronic integration with low power consumption.

Results and discussion

Device structure and basic characteristics

In order to provide a precise temperature control below RT, a micro-manipulation cryogenic probe system is adopted first in this work to study pyro-phototronic effect and photoresponse performances of the UV sensor. A digital image of the micro-manipulation probe system is shown in Fig. S1 (Supporting Information). As schematically shown in Fig. 1a, the liquid nitrogen is applied as the cryostat of the system chamber, controlling the whole system temperature ranges from 300 to 77 K. By shinning a 325 nm UV laser passing through the chamber window, as an optical stimulus, the pyro-phototronic effect and corresponding photoresponse performances of the p-Si/n-ZnO UV PD is comprehensively studied. Detailed structure of UV PD is graphically illustrated in Fig. 1b. The p-type Si wafer needs to be adequately cleaned firstly. Then, a method of magnetron sputtering is used to sputter a layer of ZnO seed for ZnO NWs grown by hydrothermal method [25,26]. Finally, a layer of indium-tin oxide (ITO) is deposited on the top of ZnO NWs array as a transparent top electrode and metal copper (Cu) is deposited on the back-side of Si wafer as a bottom electrode. The Ohmic contacts at Cu/p-Si and ITO/ZnO NWs interfaces were experimentally confirmed to eliminate the effect of contact resistance on the device performances. The detailed results are found in Fig. S2 (Supporting Information). Besides, the top and cross-section view of the sputtered ITO layer, shown in Fig. S2a-b, indicates that ITO was primarily deposited onto the tip of the uniform ZnO NWs and form a suspended top ceiling layer finally, which could effectively avoid the potential short-circuit and current leakage problems. Fig. 1c1-c2 exhibit cross-section-view and top-view scanning electron microscopy (SEM) images of the grown ZnO NWs. It can be seen from the figures that the NWs are uniform with diameters of 40–70 nm and lengths of ~2 μm). Detailed description of the fabrication process and measurement method are found in the Experimental Section.

Under 325 nm laser illumination, *I–V* characteristic curves of the self-powered p-Si/n-ZnO UV PD are measured and drawn in Fig. 1d by varying the light intensities from 2.1×10^{-6} to 9.8×10^{-4} W•cm^{-2} at 300 K, exhibiting excellent UV response and rectification characteristics at each light intensity. As well as, the output currents of the UV PD increase monotonously as increasing the light intensity, because the greater the UV intensity, the more photons are absorbed for electron-hole pairs. Fig. 1e shows the *I–t* characteristic curves of the self-powered p-Si/n-ZnO UV PD were measured under 325 nm laser illumination through an optical chopper at 1000 Hz, reflecting a uniform and repeatable photoresponse characteristic of the UV PD. More cycles of the *I–t* characteristic curve is shown in Fig. S3 (Supporting Information). Interestingly, the output current has a sharp rising peak, then reaches a stable value, followed by a falling edge appears, and finally reaches a constant value, which is quite different from traditional PDs.

To explore more physical insight, a single cycle of the *I–t* characteristics curve could be divided into four distinct stages, labelled as I, II, III and IV in Fig. 1f, to detailedly explain the influence of the pyroelectric effect based on self-powered p-Si/n-ZnO UV PD. In stage 'I', at room temperature, the UV sensors maintain a steady current in the dark state that is labeled as I_{dark}. In stage 'II', when the 325 nm UV laser is suddenly irradiated, the temperature of the ZnO NWs suddenly rises induced by the photothermal property of UV light, and a pyroelectric effect is generated, in which positive polarization charge appear at the top electrode and negative polarization charge appear at the bottom electrode. By using finite volume (FV) method based on the transient heat conduction equation [20], the corresponding temperature-time curve at the moment of turning on is calculated and shown in Fig. S4 (Supporting Information), which follows the same trend with our experimental result in stage 'II'. It can be understood from the analysis that the current (I_{py}) generated by the pyroelectric effect is consistent with the direction of the photocurrent (I_{ph}) generated by the photovoltaic effect, hence, a sharp rising peak is generated at the moment of turning on light and the output current is labeled as I_{py+ph}. In stage 'III', when the UV light is continuously irradiated, the temperature of the ZnO NWs reaches a constant value or the temperature change amount (ΔT) is equal to zero, causing the pyroelectric effect to disappear rapidly. Therefore, the output current is lowered and maintained at a stable plateau, labeled as I_{ph}. In stage 'IV', at each instant of turning off the light, the temperature is lowered that causing the direction of pyroelectric polarization to be opposite to that in stage 'II', and the photovoltaic effect disappears, causing the current to drop to a negative magnitude. When the temperature gradually decreases back to room temperature, the pyroelectric effect disappears again and the output returns to dark current.

Physical mechanisms

The physical mechanism of the pyro-phototronic effect is unambiguously elaborated in Fig. 2a–d, which corresponds to the four stages in Fig. 1f. Energy band diagram in equilibrium of p-Si/n-ZnO heterojunction is shown in Fig. 2a, indicating that the direction of the built-in electric field (E_b) is directed to Si by ZnO. At the instant of turning on the light, the temperature of ZnO NWs suddenly rises (in the nanosecond range), which give rise to a negative pyro-polarization charges at local interface of pn heterojunction

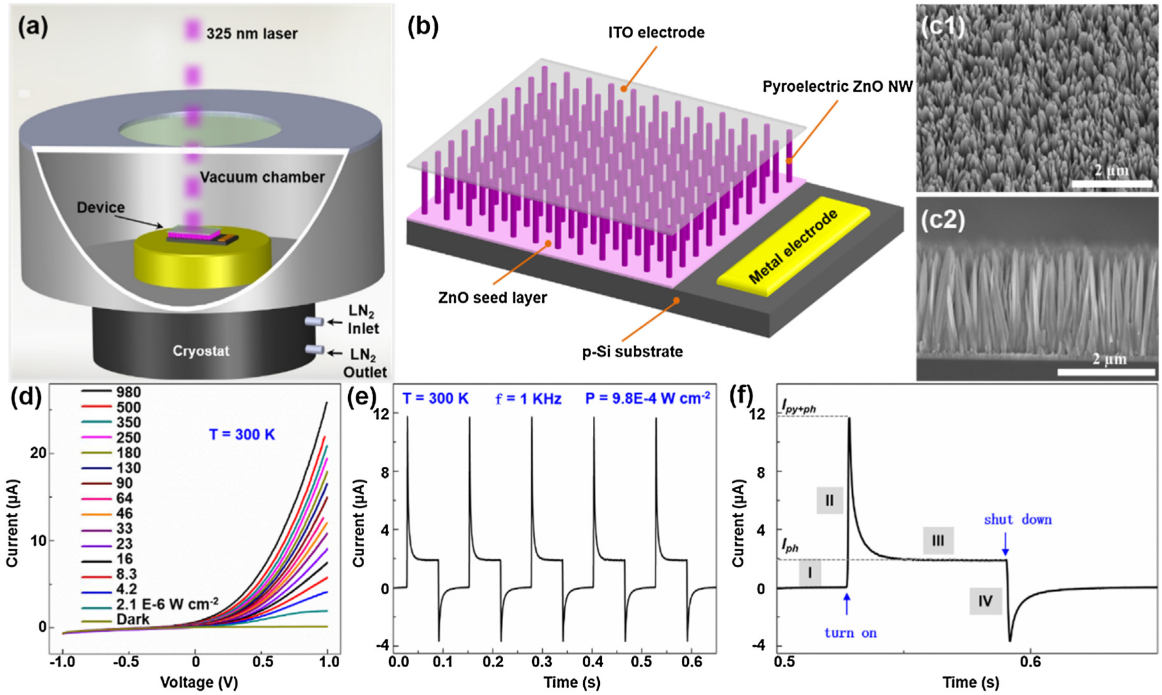

Fig. 1. Device structure and basic characterization of self-powered p-Si/n-ZnO UV sensors. **(a)** Schematic of experimental set up. **(b)** The structure of UV sensor. Top-view **(c1)** and cross-sectional **(c2)** SEM images of ZnO NWs array. **(d)** *I–V* characteristics curve of the UV sensors under dark and 325 nm laser radiation with different light intensities at T = 300 K. **(e)** *I-T* characteristics of the UV sensors under 325 nm layer illuminations with P = 9.8 × 10^{-4} W•cm^{-2} at 1000 Hz. **(f)** Enlarged drawing of a single cycle for 325 nm radiation, divided into four stages, labelled as 'I', 'II', 'III' and 'IV'.

and produce a pyroelectric electric field (E_{py}) as shown in Fig. 2b. As a result, the direction of E_{py} is consistent with E_b and is opposite to the direction of the electric field generated by the photovoltaic effect (E_{ph}). Due to the emergence of E_{py}, E_b is strengthened to some extent that accelerates the separation of photogenerated carriers and allows more photogenerated carriers to participate in the diffusion motion. For another, because E_{py} causes electrons in ZnO to move to the right, both the conduction and valence band of ZnO decrease based on Anderson's model (Fig. 2b) [27]. Therefore, the transmission of charge carriers in the heterojunction is prominently enhanced, increasing the transient output current of the UV sensors. When the UV light is stabilized, the temperature change quickly disappears, causing the pyroelectric effect to vanish; under the action of photoexcitation, the photocurrent is maintained at a constant value, as shown in Fig. 2c. Without the UV illumination, contrary to the instant of turning on the light, the temperature of the ZnO NWs decreases rapidly, resulting in a positive pyro-polarization charges in the interface of pn heterojunction. The direction of the E_{py} caused by the pyroelectric effect is opposite to the direction of the E_b of the heterojunction itself. Under the action of E_{py}, electrons will aggregate on pn-juncted interface, resulting in a decrease in the valence band and the conduction band of ZnO and forming an electron potential well, which seriously affects carriers' transport across the heterojunction [27]. In summary, the physical mechanism of the pyro-phototronic effect of self-powered p-Si/n-ZnO UV sensors has been explained in details. Since the pyroelectric effect plays an effective role in regulating the transport of carriers, the photoresponsivity of the UV sensors is improved. In order to more accurately explore the effect of pyro-phototronic effect on the performance of UV sensors, the parameter $R_i = (I_{py+ph} - I_{ph})/I_{ph}$ was introduced. The relationship between the chopping frequency and the parameter R_i is shown in Fig. 2e. The separated *I-T* curve under different chopping frequencies are shown in Fig. S5a (Supporting Information), and the corresponding I_{py+ph} and I_{ph} are extracted and plotted in Fig. S5b-c. At room temperature, R_i increases monotonically with the increase of the chopping frequency, indicating that the higher the frequency, the stronger the pyro-phototronic effect with P = 9.8 × 10^{-4} W•cm^{-2} UV illumination. Similarly, when the chopping frequency gradually increases from 0 to 1000 Hz, the response time (t_{resp}) and recovery time (t_{rec}) of the p-Si/n-ZnO UV PD show the same trend and decrease rapidly with the increase of frequency, as shown in Fig. 2f. The reason for the above phenomena are that the current generated by the pyroelectric effect is inversely proportional to Δt, that is $I_{py} \propto \Delta T/\Delta t$. This is different from the thermoelectric effect that is governed by the temperature-difference (ΔT) between the top and bottom ends/surfaces of the materials. Furthermore, a comparative experiment, by introducing the thermoelectric material TiO_2 NWs, has been designed to verify the dominant role of the pyroelectric effect in our experimental observations. Details about preparation and measurement results of the p-Si/n-TiO_2 NWs UV sensor are found in Fig. S6 (Supporting Information). Besides, the frequency dependence of the corresponding photoresponsivity R is clearly drawn in Fig. S7 (Supporting Information). The results indicate that as the chopping frequency increases, the photoresponsivity R increases monotonously. When the frequency reaches 1 K Hz, photoresponsivity R tends to reach saturation.

Performances of the UV sensor below RT

I–t characteristics curves of self-powered p-Si/n-ZnO UV PD at 77 K and 300 K are displayed in Fig. 3a–b by varying the UV light intensities from 1.6 × 10^{-5} to 9.8 × 10^{-4} W•cm^{-2}. For each individual cycle, as shown in Fig. 3a–b, there are a sharp rising peak (I_{py+ph}) caused by an increase in temperature of ZnO NWs, a steady plateau (I_{ph}), a falling peak induced by pyroelectric effect at the instant of turning off the light and a maintenance level (I_{dark}). At 77 K and 300 K, it is found that as the light intensity increases, more photons are absorbed by the ZnO material, resulting in a monotonous increase in the photocurrent (I_{ph}) and the

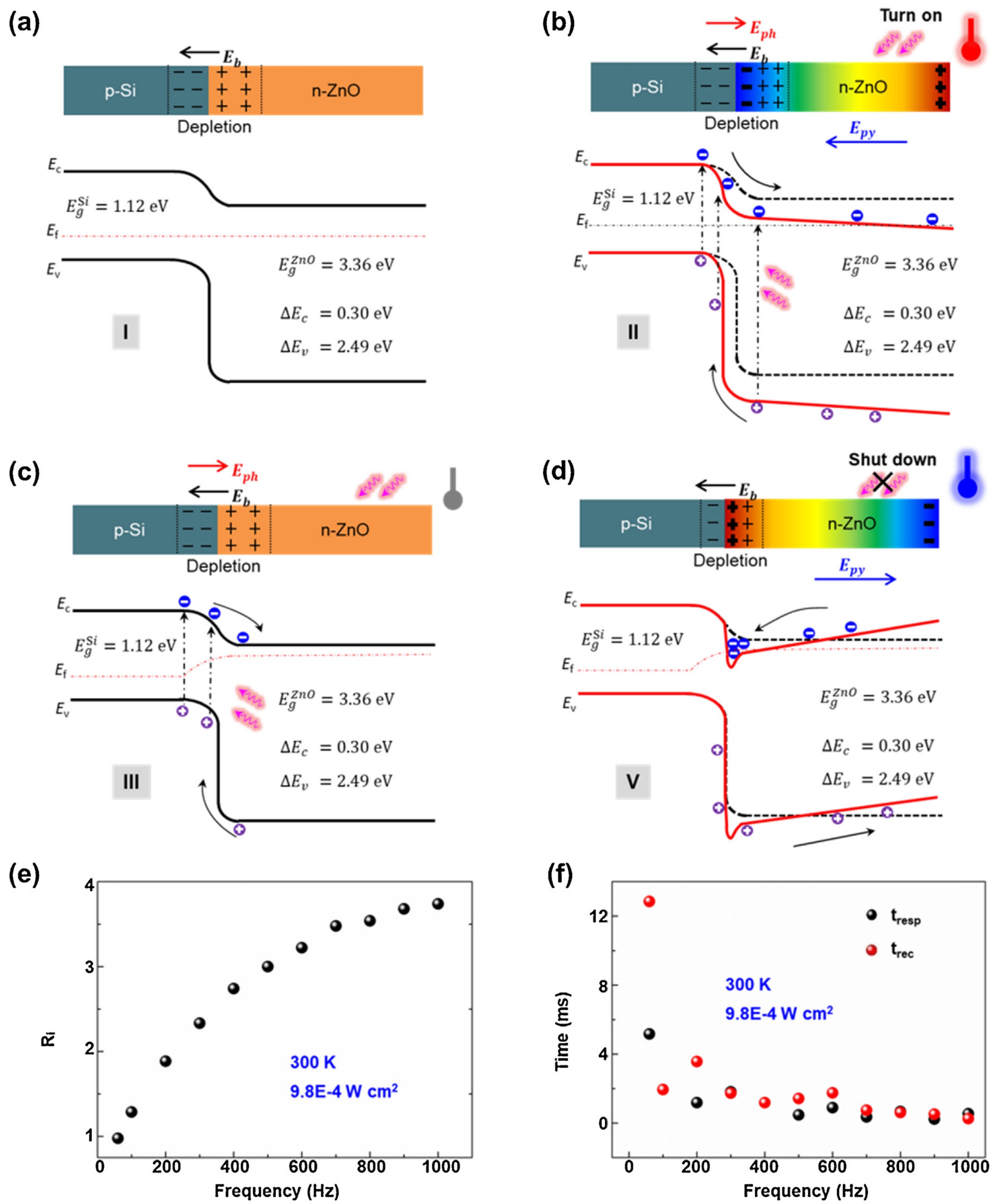

Fig. 2. Band diagrams of p-Si/n-ZnO heterojunction and the influence of the chopping frequency on p-Si/n-ZnO UV sensors. **(a)** as dark **(b)** the moment of turning on **(c)** as continuous UV illumination and **(d)** as turning off light. **(e)** Parameter R_i enhancement under different chopping frequencies. **(f)** Response and recovery time decrease under different chopping frequencies.

pyroelectric current (I_{py}). Detailly, upon P = 9.8 × 10^{-4} W•cm^{-2} UV radiation, *I–t* characteristics curve of self-powered p-Si/n-ZnO UV sensors at different temperature range from 77 to 300 K is extracted and drawn in Fig. 3e to prove the effect of temperature on the output current. It is noteworthy that the dark current of the *I-T* response curve under each condition in Fig. 3a–b and e have the same order of magnitude of 10^{-9}A with negligible fluctuation. The separated *I-T* curve under each condition are found in Fig. S8 (Supporting Information). The corresponding current responses I_{py+ph} and I_{ph} of the self-powered p-Si/n-ZnO UV sensors are integrally studied in Fig. 3c–d at different UV light intensities and temperatures, in order to illustrate the enhancement of the output currents (I_{py+ph}) by the pyro-phototronic effect. Obviously, both I_{py+ph} and I_{ph} increase monotonically with increasing light intensity. However, changes in I_{py+ph} and I_{ph} are not monotonic with temperature changes, as there are two mechanisms that play a competing role. The relevant current responses I_{py+ph} and I_{ph} of the self-powered p-Si/n-ZnO UV PD under different temperature range from 77 K to 300 K with different light intensities are methodically studied and formulated in Fig. 3f–g to manifest the impact of low temper-

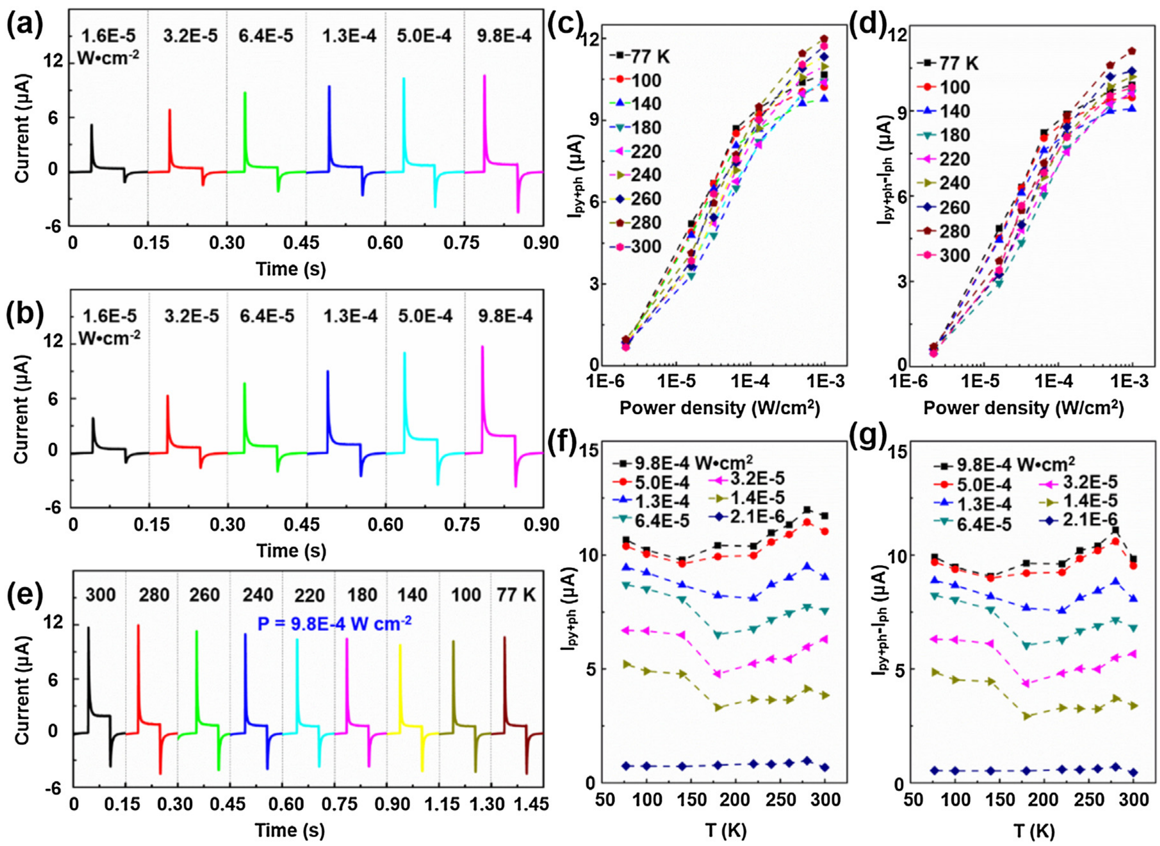

Fig. 3. Current response of self-powered p-Si/n-ZnO UV sensors under different temperatures and UV light intensities. *I–t* characteristics of UV sensors at 77 K **(a)** and 300 K **(b)**. Output current (I_{py+ph}) **(c)** and pyroelectric current (I_{py}) **(d)** at different light intensities ranging from 1×10^{-6} to 1×10^{-3} W•cm^{-2} under 325 nm UV laser radiation with different temperatures. **(e)** *I–t* characteristics of UV sensors with temperatures ranging from 77 to 300 K at P = 9.8×10^{-4} W•cm^{-2}. Output current (I_{py+ph}) **(f)** and pyroelectric current (I_{py}) **(g)** with temperatures ranging from 77 to 300 K under different light intensities.

ature environment on the pyro-phototronic effect. Firstly, as the overall temperature drops, the light-self-induced temperature difference (ΔT) increases, resulting in a gradual increase in the current (I_{py}), $I_{py} \propto \Delta T/\Delta t$. Secondly, under the action of low temperature (77 to 290 K), the carrier concentration tends to increase exponentially due to the continuous ionization of the donor or acceptor impurities, and the carrier mobility increases due to the decreasing scattering of ionized impurities. Therefore, at low temperatures, the conductivity increases with increasing temperature. At room temperature (20 to 30 °C), the carrier concentration is constant because the donor or acceptor impurities have been completely ionized, but the conductivity will deteriorate due to the decrease in carrier mobility with increasing temperature. When the temperature keeps rising, the phonon scattering caused by the increase in lattice vibration is continuously enhanced. When the temperature range is 77 to 180 K, the pyro-phototronic effect dominates, causing I_{py+ph} and I_{ph} to increase monotonically with decreasing temperature. However, the increase in carrier concentration dominates, resulting in I_{py+ph} and I_{ph} increase monotonically with increasing temperature in the temperature range of 180 to 290 K.

The defined parameter $R_i = (I_{py+ph} - I_{ph})/I_{ph}$ is used to reflect the effect of pyro-phototronic effect on the output current of pn-juncted UV sensors at different temperatures and light intensities, as plotted in Fig. 4. The relationship between R_i and UV light intensity at different temperatures, and the relationship between R_i and temperature at different UV light intensities are studied and shown in Fig. 4a–b. As the increases of the light intensity, it leads to an increase in I_{ph}, which also leads to an increase in the amount of temperature change on the ZnO NWs. Therefore, at most light intensities (less than 1×10^{-4} W•cm^{-2}), the parameter R_i initially increases, as illustrated in Fig. 4a. However, as the light intensity continues to increase, I_{ph} increases more than I_{py}, resulting in a decrease in R_i. According to Fig. 4b, under different light intensities, the value of R_i will be different. In the ultra-low temperature section (less than 150 K), R_i has the maximum value at the light intensity of 6.4×10^{-5} W•cm^{-2}, and R_i shows the maximum value when the light intensity is 1.3×10^{-4} W•cm^{-2} in the low temperature range (150–300 K). The relationship between R_i and light intensity is inconsistent in different temperature ranges, which indicates that temperature has a great influence on pyroelectric effect, carrier concentration, carrier mobility and the like. However, for each light intensity, the R_i of the ultra-low temperature section (less than 150 K) is larger than the low temperature section (150–300 K), which proves that the lower the temperature, the more favorable the regulation of the pyroelectric effect. The reason for this phenomenon is that under the same UV irradiation, the lower the ambient temperature, the greater the amount of temperature change produced. At the same time, due to the influence of temperature on carrier concentration and mobility, I_{ph} will decrease with the decrease of temperature under the same light intensity. In short, when the temperature and the light intensity change simultaneously, the two play a competitive role in the regulation of the output signal of the UV sensors. In order to calculate the transferred charge, Q_{pyro} (is defined as the integration of I above the reference number I_{ph} and t), Fig. 4c shows the *I-T* characteristic curve for a single cycle. The relationship between temperature, light intensity and transferred charge because of the pyro-phototronic effect are summarized and shown in Fig. 4d in the form of a three-dimensional plot to illustrate that a higher number of Q_{pyro} is acquired under a higher temperature and stronger

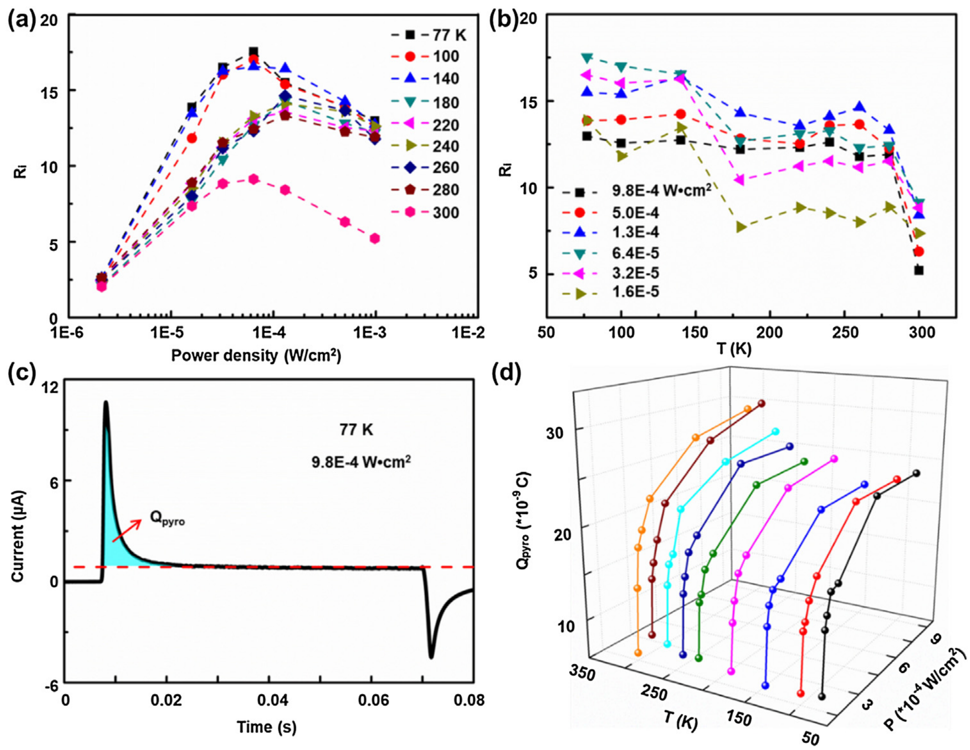

Fig. 4. Temperature and power dependence of effectively transferred charges Q_{pyro} and parameter R_i. R_i under different light intensities **(a)** and temperatures **(b)**. **(c)** The derivation of the transferred charges. **(d)** 3D plot depicting the dependence of transferred charges on light intensities and temperatures.

UV illumination. The detailed results about temperature and light intensity dependences of the Q_{pyro} are found in Fig. S9 (Supporting Information).

Performances of the UV sensor above RT

The pyro-phototronic effect in the fabricated UV PD at the temperature condition above RT is further studied on a hot plate, as schematically shown in Fig. 5a. Two-dimensional plots obtained by studied the photocurrent responses (I_{py+ph}) to the pyro-phototronic (Fig. 5b) and the photocurrent responses (I_{py}) to the pyroelectric effect (Fig. 5c) at different temperatures range from 25 to 85 °C with different light intensities. According to the measured experimental results, the analysis was performed from two levels of room temperature (20 to 30 °C) and high temperature (more than 30 °C). At room temperature, the amount of temperature change (ΔT) will decrease as the temperature of the system increases, so the pyroelectric effect will be attenuated. On the other hand, as the temperature of the system increases, the phonon scattering gradually increases, resulting in a decrease in carrier mobility, so the conductivity will decrease as the temperature increases. For the above two reasons, below 30 °C, I_{py+ph} and I_{py} decrease with increasing temperature.

In the high temperature range, firstly, the higher the temperature, the stronger the phonon scattering and the lower the mobility; secondly, the intrinsic excitation starts to work at high temperatures, resulting in an increase in carrier concentration, which increases the amount of transferred charges; Finally, the current (I_{py}) generated by the pyroelectric effect is proportional to the amount of change in temperature per unit time, $I_{py} \propto \Delta T/\Delta t$, leading to I_{py} not monotonic with increasing temperature. A mutually competing mechanism is formed among these three processes, resulting in I_{py+ph} decrease followed by increases, as the temperature continues to rise.

Parameter R_i of the UV PD is calculated to represent the effect of pyro-phototronic effect on the output signal of pn-juncted UV sensors at different temperatures and light intensities, as plotted in Fig. 5d. As the temperature rises from 25 to 85 °C, R_i exhibits a local maximum. Within this temperature range (25 to 45 °C), R_i shows an increasing trend due to the reduction of photocurrent caused by the enhanced carriers scattering. The temperature T_0 where the maximum R_i appears at approximately 45 °C. As further increasing the temperature from 35 to 45 °C, the intrinsic excitation occupies a dominant position, resulting in an increase in carrier concentration and a sharp decrease in R_i. However, as the temperature continues to increase, the decrease in carrier mobility and the increase in carrier concentration have the same effect on the current, R_i tends to a stable value with temperature.

Conclusion

In conclusion, by analyzing the photoresponse performances of p-Si/n-ZnO NW UV PD at different temperatures, the relationship between temperature and the pyro-phototronic effect is obtained in the UV sensors. At a lower environment temperature, the temperature change (ΔT) caused by UV irradiation changes more than that at room temperature, resulting in a more pronounced pyroelectric effect, which in turn helps to reduce the response time of the UV PD. At 77 K, the current response of the UV PD is significantly improved by over 1304%, while at RT the current response is only increased by 532.6% induced by the pyroelectric effect. Under the temperatures above RT, the UV PD functions well even the temperature is elevated to 85 °C from RT. There is the weakening of the pyroelectric effect and the influence of the lattice vibration on the device, but the carrier concentration and activity are also significantly increased at a higher environment temperature. When the temperature is at 85 °C, the current-response of the sensors is significantly enhanced by more than 567% due to the pyro-phototronic effect. In addition, using the energy band structure diagram, the

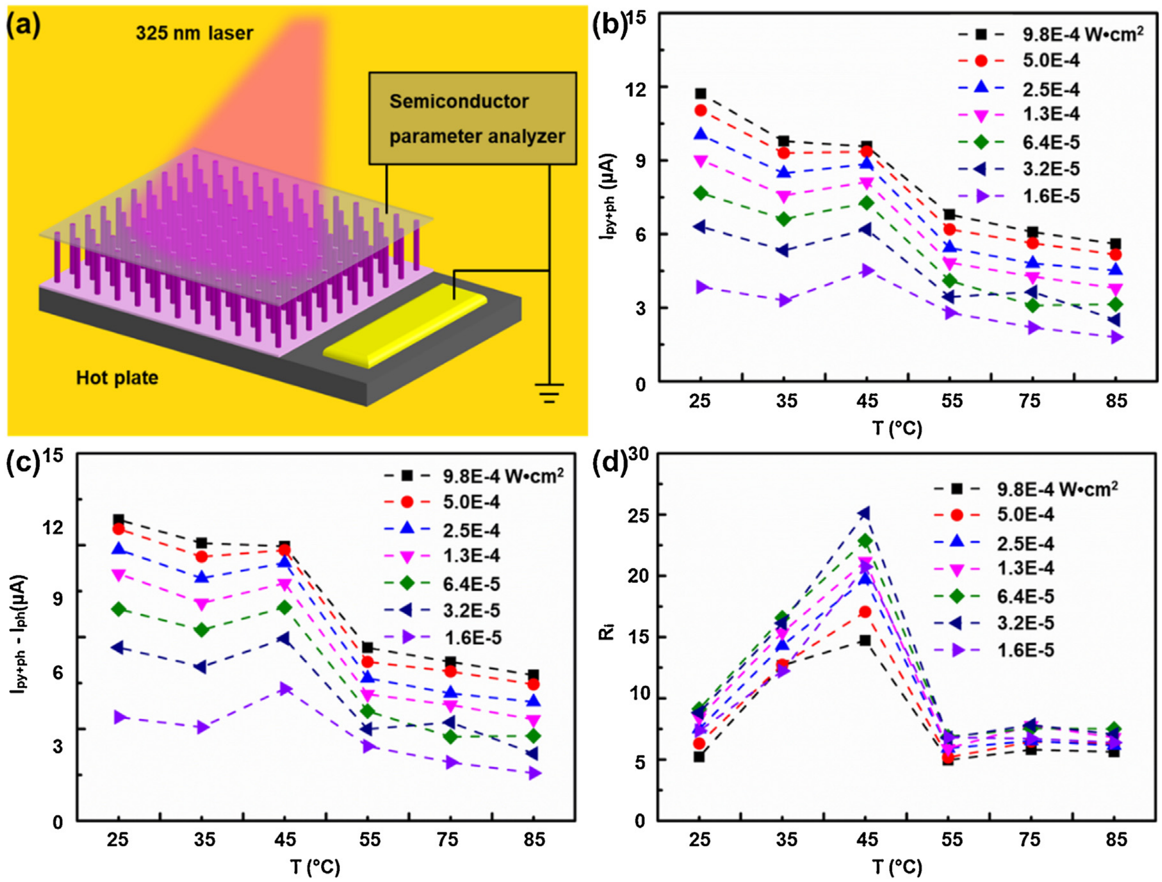

Fig. 5. Photo-response of self-powered p-Si/n-ZnO UV sensors under different temperatures and light intensities. **(a)** Schematic of heated experimental set up. **(b), (c)** Output current (I_{py+ph}) and pyroelectric current (I_{py}) with temperatures ranging from 25 to 85 °C under different light intensities. **(d)** Parameter R_i with the temperatures ranging from 25 to 85 °C under different light intensities.

working mechanism of the pyro-phototronic effect is elaborated. The relationship between the transferred charge generated by the pyroelectric effect and the light intensities and temperature is also discussed. The work deeply studies the temperature dependence of the pyroelectric effect, and has guiding significance for practical applications in ultrafast photo-sensing, optothermal detection and so on.

Experimental section

ZnO NWs growth and device fabrication

Commercially purchased 500 μm-thick p-type Si(100) wafer, with a conductivity of 1–10 Ω cm, was cut into 1 × 1 cm^2 pieces and utilized as the substrate for ZnO NWs growth. Before growth, a layer of 100 nm-thick ZnO seed was deposited onto the p-Si substrate using radio-frequency (RF) magnetron sputtering method, under the RF power of 120 W for 30 min.. 250 ml mixed solution of 0.02 mM $Zn(NO_3)_2$ and 0.02 mM hexamethylenetetramine was prepared and utilized for hydrothermal growth of the ZnO NWs. The ZnO seed coated p-Si pieces were put upside down on the solution for a growth time of 1 h at the temperature of 90 °C in a vacuum oven. In order to better control the morphology, diameter and length of ZnO NWs, 10 mL ammonium hydroxide with the concentration of 28% was also mixed into the growth solution. After a natural cooling of the solution, the obtained ZnO NWs array on p-Si was carefully taken out and gently washed by ethanol and distilled water, followed by a vacuum drying process at 60 °C for 1 h. To fabricate the self-powered UV sensor, a 120 nm thick of ITO layer and 100 nm Cu layer were deposited onto top surface of the ZnO NWs array and the back-side of the p-Si substrate as the top and bottom electrode, respectively.

Performances measurements of the self-powered UV sensors

The I–V and I–T characteristics of the fabricated self-powered UV sensors were measured and collected by a customized computer-controlled measurement system consists of a function generator (Stanford Research system DS345) and low-noise current preamplifier (Stanford Research system SR 570). A He-Cd laser with wavelengths of 325 nm was used as the excitation laser source in this work for characterizing the photoresponse performances of the self-powered UV sensors.

Declaration of Competing Interest

The authors declare no competing financial interest.

Acknowledgements

This research was supported by the National Key R & D Project from Minister of Science and Technology (2016YFA0202704), and the Hightower Chair foundation. This research was also supported by the National Natural Science Foundation of China (Grant No.11804103), Guangdong Natural Science Foundation for Distinguished Young Scholars (Grant No. 2018B030306048).

Appendix A. Supplementary data

Supplementary material related to this article can be found, in the online version, at doi:https://doi.org/10.1016/j.nantod.2019.100798.

References

[1] Q. Wu, L.X. Gong, Y. Li, C.F. Cao, L.C. Tang, L.B. Wu, L. Zhao, G.D. Zhang, S.N. Li, J.F. Gao, Y.J. Li, Y.W. Mai, ACS Nano 12 (2017) 416–424.
[2] S. Choi, N. Kim, H. Cha, R. Ha, Sensors 9 (2009), 7970-1987.
[3] M.C. Carotta, G. Martinelli, L. Crema, C. Malagù, M. Merli, G. Ghiotti, E. Traversa, Sens. Actuators B: Chem. 76 (2001) 336–342.
[4] B. Vrana, I.J. Allan, R. Greenwood, G.A. Mills, E. Dominiak, K. Svensson, J. Knutsson, G. Morrison, TrAC Trends Analy. Chem. 24 (2005) 845–868.
[5] T. Kolbe, A. Knauer, C. Chua, Z. Yang, S. Einfeldt, P. Vogt, N.M. Johnson, M. Weyers, M. Kneissl,Appl. Phys. Lett. 97 (2010), 171105.
[6] J. Witt, K. Krebber, J. Demuth, L. Šašek, International Workshop on Biophotonics, IEEE, 2011, pp. 1–3.
[7] W. Tian, C. Zhang, T.Y. Zhai, S.L. Li, X. Wang, J.W. Liu, X. Jie, D.Q. Liu, M.Y. Liao, Y. Koide, D. Golberg, Y. Bando, Adv. Mater. 26 (2014) 3088–3093.
[8] G. Li, M. Suja, M. Chen, E. Bekyarova, R.C. Haddon, J. Liu, M.E. Itkis, ACS Appl. Mater. Interfaces 9 (2017) 37094–37104.
[9] M. Spies, M.I. Den Hertog, P. Hille, J. Schörmann, J. Polaczyński, B. Gayral, M. Eickhoff, E. Monroy, J. Lähnemann, Nano Lett. 17 (2017) 4231–4239.
[10] Y. Hu, J. Zhou, P.H. Yeh, Z. Li, T.Y. Wei, Z.L. Wang, Adv. Mater. 22 (2010) 3327–3332.
[11] T.V. Tam, S.H. Hur, S.C. Jin, W.M. Choi, Sens. Actuators A Phys. 233 (2015) 368–373.
[12] H.S. Wu, W.W. Zhang, J.J. Wu, Y.W. Chi, ACS Appl. Mater. Interfaces 11 (2019) 16713–16719.
[13] T. Journot, V. Bouchiat, B. Gayral, J. Dijon, B. Hyot, ACS Appl. Mater. Interfaces 10 (2018) 18857–18862.
[14] J.J. Yu, K. Javaid, L.Y. Liang, W.H. Wu, Y. Liang, A.R. Song, H.L. Zhang, W. Shi, T.C. Chang, H.T. Cao, ACS Appl. Mater. Interfaces 10 (2018) 8102–8109.
[15] S. Dhar, P. Chakraborty, T. Majumder, S.P. Mondal, ACS Appl. Mater. Interfaces 10 (2018) 41618–41626.
[16] W. Yang, K. Hu, F. Teng, J. Weng, Y. Zhang, X. Fang, Nano Lett. 18 (2018) 4697–4703.
[17] G. Heiland, H. Ibach, Solid State Commun. 4 (1966) 353–356.
[18] C.C. Hsiao, S.Y. Yu, Sensors 12 (2012) 17007–17022.
[19] C.C. Hsiao, S.W. Huang, R.C. Chang, Sens. Mater. 24 (2012) 421–441.
[20] Z. Wang, R. Yu, C. Pan, Z. Li, J. Yang, F. Yi, Z.L. Wang, Nat. Commun. 6 (2015) 8401.
[21] X.F. Wang, R.M. Yu, C.Y. Jiang, W.G. Hu, W.Z. Wu, Y. Ding, W.B. Peng, S.T. Li, Z.L. Wang, Adv. Mater. 28 (2016) 7234–7242.
[22] W.B. Peng, R.M. Yu, X.F. Wang, Z.N. Wang, H.Y. Zou, Y.N. He, Z.L. Wang, Nano Res. 9 (2016) 3695–3704.
[23] Z. Wang, R. Yu, X. Wen, Y. Liu, C. Pan, W. Wu, Z.L. Wang, ACS Nano 8 (2014) 12866–12873.
[24] Z.N. Wang, R.M. Yu, X.F. Wang, W.Z. Wu, Z.L. Wang, Adv. Mater. 28 (2016) 6880–6886.
[25] Y. Liu, A. Das, S. Xu, Z. Lin, C. Xu, Z.L. Wang, A. Rohatgi, C.P. Wong, Adv. Energy Mater. 2 (2012) 47–51.
[26] Y. Xie, M. Madel, Y. Li, W. Jie, B. Neuschl, M. Feneberg, K. Thonke,J. Appl. Phys. 112 (2012), 123111.
[27] Y. Liu, S. Niu, Q. Yang, B.D. Klein, Y.S. Zhou, Z.L. Wang, Adv. Mater. 26 (2014) 7209–7216.

Jianqi Dong received her bachelor's degree from Henan Normal University. Now she is a postgraduate student in the Xingfu Wang's Group of South China Normal University. Her research focuses on the growth of nanomaterials, GaN based LEDs and HEMTs.

Zhengjun Wang obtained bachelor degree and Ph.D. both in physics from Henan Normal University and West Virgnia University, respectively. He is currently a Postdoctoral Fellown Prof. Zhong Lin Wang's group at Georgia Institute of Technology, his research interests focus on fabrication of nanoelectronics devices and triboelectric nanogenerators.

Xingfu Wang received his Ph.D degree from South China Normal University (SCNU), with awards of Excellent Ph.D Dissertation, Top-ten Excellent Academic Paper in SCNU and National Scholarship for Graduate Students from Chinese Ministry of Education. From 2014–2017, he worked as a visiting scholar and research engineer in Prof. Zhong Lin Wang's group at Georgia Tech. He now is a professor, Outstanding Young Scholar at SCNU, Guangzhou, China. His research interests include epitaxial growth of III-Nitride planar/nano-structures by Metal-Organic Chemical Vapor Deposition (MOCVD); GaN-based light-emitting-diode (LEDs) and high-electron-mobility-transistor (HEMTs); Piezotronics/Piezo-photonics.

Zhong Lin Wang received his Ph.D. from Arizona State University in Physics. He now is the Hightower Chair in Materials Science and Engineering, Regents' Professor, Engineering Distinguished Professor and Director, Center for Nanostructure Characterization, at Georgia Tech. Dr. Wang has made original and innovative contributions to the synthesis, discovery, characterization and understanding of fundamental physical properties of oxide nanobelts and nanowires, as well as application of nanowires in energy sciences, electronics, optoelectronics and biological science. His discovery and breakthroughs in developing nanogenerators established the principle and technological road map for harvesting mechanical energy from environment and biological systems for powering personal electronics His research on selfpowered nanosystems has inspired the worldwide effort in academia and industry for studying energy for micro-nano-systems, which is now a distinct disciplinary in energy research and future sensor networks. He coined and pioneered the field of piezotronics and piezo-phototronics by introducing piezoelectric potential gated charge transport process in fabricating new electronic and optoelectronic devices. Details can be found at: http://www.nanoscience.gatech.edu.